Title: **Dynamic behavior of a power re-circulating gear test rig including periodic variation of mesh stiffness and static transmission error**

Authors: **M. Abruzzo, M. Beghini, C. Santus, S. Manconi**

DOI Link: https://doi.org/10.1016/j.mechmachtheory.2021.104247

Dynamic behavior of a power re-circulating gear test rig including periodic variation of mesh stiffness and static transmission error

M. Abruzzo[a,*], M. Beghini[a], C. Santus[a], S. Manconi[b]

[a]*DICI, Department of Civil and Industrial Engineering, University of Pisa, Italy.*
[b]*AM Testing Srl, Pisa (PI), Italy.*

Abstract

We characterized the dynamic behavior of a pair of high performance aeronautical gears which are part of a complex transmission system. The gear pair was tested using a mechanical recirculating power test rig designed to simulate the severe operating conditions of transmitted torque and angular speed. The test rig and the most important phenomena that influence its dynamic behavior are described. A (static) finite element model, developed to calculate the input parameters for the dynamic analysis of the tested gears, is also presented. Using the results of the FE model, we developed a lumped dynamical model with which it is possible to reproduce the most significant dynamic phenomena of the test rig. We characterized the behavior of the test rig focusing on the actual loads transmitted by the tested gears. The dynamic model was validated by comparing its results with the experimental outcomes in various test conditions. The comparison highlights the limitations of the design procedures based on common standards for assessing the dynamic overload experienced by heavy-duty gear transmission systems.

Keywords: Gearing and transmission; Spur gears; Dynamics of machinery; Dynamic overload; Nonlinear vibrations

*Corresponding author: Michele Abruzzo
Ph. +39 392 617 1705
Email address: michele.abruzzo@phd.unipi.it (M. Abruzzo)

Nomenclature

$k_m(t)$	Meshing stiffness
c_m	Meshing damping
b	Gear backlash
$e(t)$	Static Transmission Error
R_{bp}	Pinion base radius
R_{bg}	Gear base radius
θ_p	Pinion rotation
θ_g	Gear rotation
$\theta(0)$	Initial angular displacement applied
I_p	Pinion moment of Inertia
I_g	Gear moment of Inertia
$F(t)$	Restoring meshing force
$u(t)$	Relative displacement along the line of contacts
ε	Contact ratio
T	Meshing period
$\bar{K}$	Midrange of the meshing stiffness
M	Static torque applied to the tested gears
K_V	Dynamic overload factor of mesh force
v	Deviation from the standard involute profile
ϕ	Involute roll angle
α	Polar angle
ζ	Damping ratio of the engaging gears
f_{mesh}	Meshing frequency of the tested gears

1. Introduction

The demand of high performance and weight reduction for power transmissions, particularly in aeronautical applications, has led to the development and experimental validation of sophisticated models for evaluating the static and dynamic behavior of gears.

Özgüven and Houser [1] reviewed the models developed to describe the dynamic of transmission systems up to the 1990s. Wang et al. [2] discussed several critical aspects of these dynamic models with particular regard to their nonlinearities.

These two studies demonstrated that the geometrical properties of the tooth, particularly modifications to the profiles, significantly affect the dynamics of gear driven systems. For spur gears, Liou et al. [3] studied the effect of the contact ratio and Kuang and Lin [4] derived an analytical formulation to model the dynamic behavior including the meshing stiffness variation during the tooth engagement and the geometrical errors of the tooth profiles. The effects of the tooth tip relief and of several profile modifications have been quantified [5, 6, 7, 8, 9]. Other research groups [10, 11] studied the effects of tooth surface micro-geometrical features. Gregory et al. [12] proposed and applied an innovative optical method to experimentally quantify the static transmission error in spur gears.

Cai and Hayashi [13] studied the dynamics of spur gears and derived a formulation to evaluate the meshing stiffness that was verified by measurements. Hichimaru and Hirano [14] investigated the dynamic behavior of heavy-loaded spur gears (high torque and low speed) in order to identify possible causes of failure at that regime. Amabili and Rivola [15], Theodossiades and Natsvias [16] investigated the steady state response and the dynamical stability of spur gears by developing and applying a model with a single degree of freedom that included a time-varying meshing stiffness and the static transmission error.

Teeth separation and the possible back-side impact can also be induced by gear dynamics. Separation of contact between meshing gear teeth can be produced in the presence of gear backlash, which is defined by the clearance between profiles of mating gears teeth that are not in contact, and this separation was observed in particular meshing conditions (typically at low torque and high speed). Eritenel and Parker [17] studied mesh non-linear dynamics and partial contact loss in helical gear pairs using a lumped parameter model. Sakaridis et al. [18] investigated the inertial effect of individual teeth on spur gear dynamics. Their results indicated that modeling the single tooth dynamics in scenarios involving gears with low numbers of teeth or low applied torque is important in order to identify contact loss or chaotic motions. Xiang et al. [19] proposed an improved model of the contact force for gear systems by separating the condition of common drive-side meshing contact and that of back-side meshing contact with collisions. The model included the estimate of the energy transferred as a

consequence of the impact. Zhu et al. [20] investigated the influence of the backlash on the dynamic behavior of encased differential planetary gear trains with multibacklash and time-varying mesh stiffness. Shi et al. [21] provided a theoretical framework for the optimization of gears by analyzing teeth separation, drive-side and back-side tooth meshing contacts. They used a lumped parameter model that includes a time-varying meshing stiffness, time-varying friction, load distribution, and static transmission error. Backlash was successfully employed.

Bending-torsional coupling also affects the dynamics of gear transmissions. This coupling has to be taken into account when the bending compliance of the shafts produces displacements at the tooth comparable to those produced by the deformation of the gears and the torque of the shafts. Wang et al. [22] characterized the bending-torsional coupling of a multi-degree of freedom spur gear system, and Su et al. [23] developed a mathematical model to study the bending–torsional–axial coupling of mixed gear trains.

We developed a power re-circulating test rig to assess high precision heavy-duty aeronautical gears. We then modeled the rig in order to accurately analyze the dynamic phenomena of the transmission under several regimes. The model was verified by comparing its outcomes with several operating parameters directly measured on the rig. A lumped parameter model with an appropriate number of degrees of freedom was demonstrated to be sufficiently accurate to numerically reproduce the main measured quantities, provided that the time-varying mesh stiffness, the static transmission error, and the gear backlash are taken into account.

The nonlinear equations of motion containing time dependent parameters were numerically integrated to obtain the dynamic response of the system while simulating the tests. The calculated natural frequencies of the rig were compared with the experimental response of the system. Given that a good agreement was found, the modal analysis based on the classical eigenvalue approach was validated. These analyses correctly indicated potentially dangerous operating conditions (torques and speeds) for the tested gears and for the rig components. However, one of the main purposes of the present work was to calculate the dynamic overload factor of the tested gears (usually called K_V). This factor is defined as the ratio between the effective maximum meshing force (at the operative speed) and the static value (at low speed). Some tests, in which steady-state conditions were reached and maintained, were thus performed. Several signals measured and recorded were directly compared with the equivalent quantities calculated by the model. Consequently, an experimental validation of K_V was obtained. In several regimes the dynamic effects were found to significantly increase the meshing force. Even under steady state conditions, the loads predicted by the dynamic factor K_V were underestimated.

2. Description of the test rig and of the tested gears

A mechanical power re-circulating test rig [24] was developed in collaboration with partners(AM Testing and the University of Pisa) for testing high-performance aeronautical gears. The rig can perform a wide spectrum of tests by setting and controlling, for example, the applied torque, rotational speed, type of lubricant and its flow rate and temperature. The maximum values of torque and speed applicable to the test articles are 500 Nm and 18000 rpm, respectively. The circulating power (transmitted to rather small spur gears) can be as large as 1 MW.

Mechanical power re-circulation was obtained by adopting the arrangement shown in figure 1. The test rig has two main sections: i) the test section, which includes the couple of gears under test with their supports; and ii) the slave section, which has two independent actuation systems that apply the required rotational speed and torque are applied to the gears under test. The torque is obtained by means of a linear actuator (indicated as "Servo" in Figure 1) which moves one of the two engaging helical gears (with helix angles with opposite signs) connected to the same shaft. The relative angular displacement of the two helical gears generates the torque applied to the elements of the rig. The angular speed is produced and maintained by an electric motor which compensates for the mechanical losses of the whole system. The slave section was designed to achieve nominally infinite life for all its components. Consequently, the components of this section are particularly precise and stiff, and only the tested gears produce a significant contribution to the vibration of the rig.

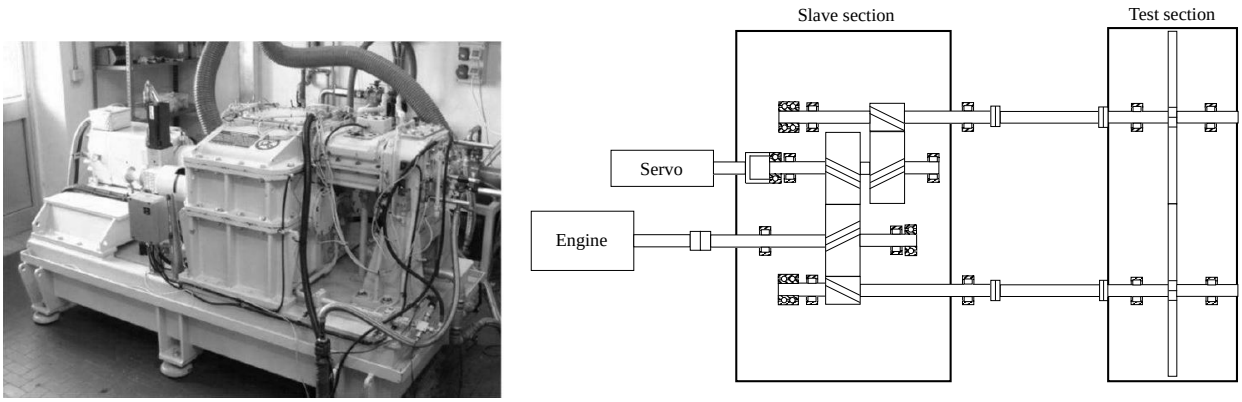

(a) (b)

Figure 1: Power re-circulating gear test rig. (a) The test rig. (b) Two-dimensional scheme and general layout (not to scale).

The rig is instrumented to measure and record several quantities. The torque transferred by the tested gears is redundantly measured on each of the shafts by two independent torquemeters. The tested gears are also equipped with a set of three strain gauges (Figure 2 b,c), glued at the face width center in the root of three teeth. With this arrangement, the strains at the tooth base can be measured and the engaging forces can be directly deduced under any test conditions.

The tested gears are made of steel and are typical components of gearboxes or power trains for aeronautical applications. Spur gears with different meshing parameters can be tested. In the present paper, the base radius of the gears tested is equal to 64.5 mm. The tooth width (measured in the hoop direction at the pitch point) is 3.0 mm. The involute tooth profile is corrected by applying a tip relief (Figure 2 a), which starts at the pitch point. The relief v is defined in the direction normal to the involute tooth profile and reaches the maximum value of $v_{\max}$ at the tooth tip.

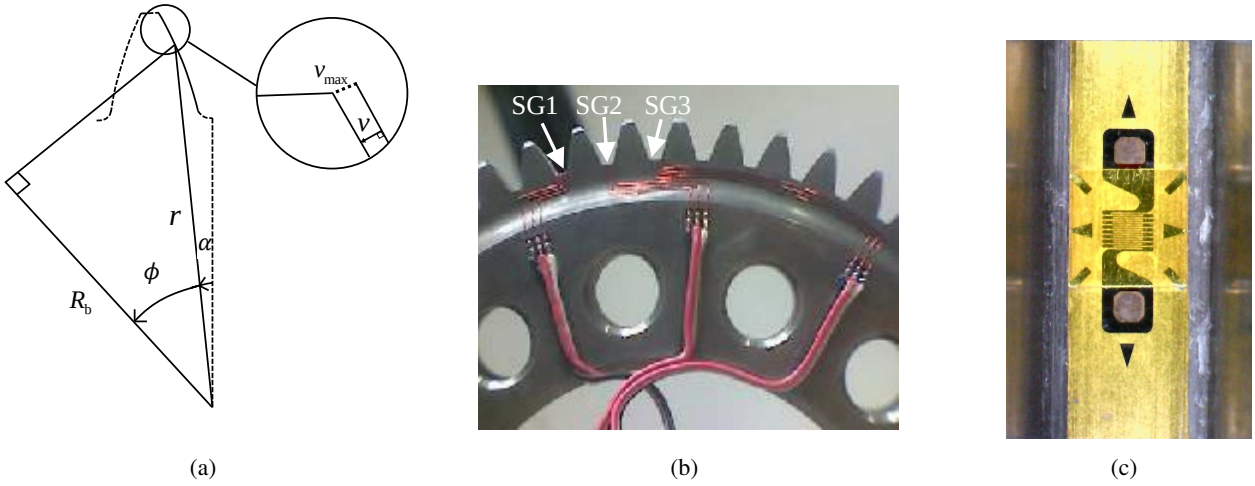

(a) (b) (c)

Figure 2: Tested gears and their instruments. (a) Detail of the tip relief: v indicates the difference between the modified profile and the nominal involute and is expressed by a parabolic function of the roll angle ϕ. α is the polar angle, measured starting from a vertical axis. (b) Strain gauges on the roots of three teeth. (c) Example of strain gauge positioning.

2.1. Measurement of the dynamic overload factor

The signals of the three strain gauges (Figure 2 b,c) are acquired with a sampling rate of 100 kHz. Strain gauge signals are used for identifying the dynamic overload factor of mesh force K_V, i.e. the ratio between the maximum force transmitted by the meshing teeth and the nominal force. When the test gears rotate at a low rotational speed (typically below a meshing frequency, f_{mesh}, of 140 Hz) under constant torque the dynamic effects are negligible, and the strain gauges directly measure the force exerted when the transmission operates in static conditions.

After the transient condition, when the operational speed of the gears has been reached, the strain gauge signal usually produces more intense peak values. This is a consequence of the vibrations induced by the elasticity during transmission. Since the three signals are the same (Figure 3), any one of them can be used to calculate the dynamic overload factor K_V in any testing condition. As an example, Figure 4 shows the signals used to quantify the dynamic overload factor at a meshing frequency of 6533 Hz. Under that regime $K_V = 1.36$.

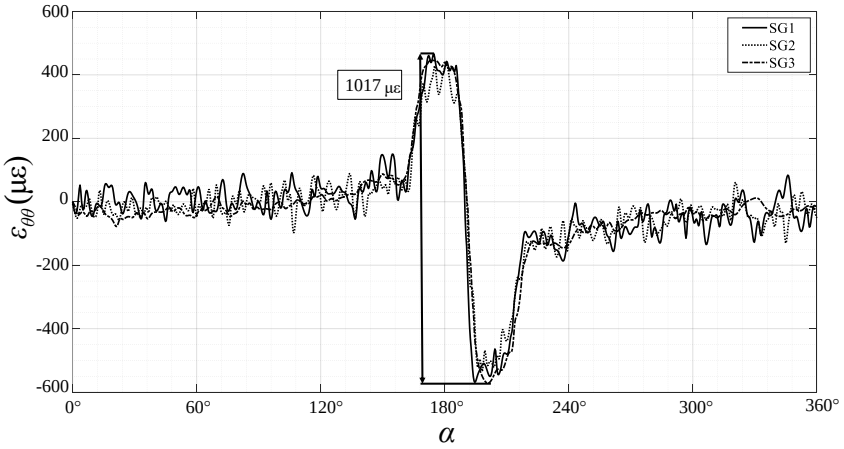

Figure 3: Signals of the static conditions of the transmission obtained by the strain gauges on the tooth fillet at a meshing frequency of 140 Hz and a torque of 150 Nm.

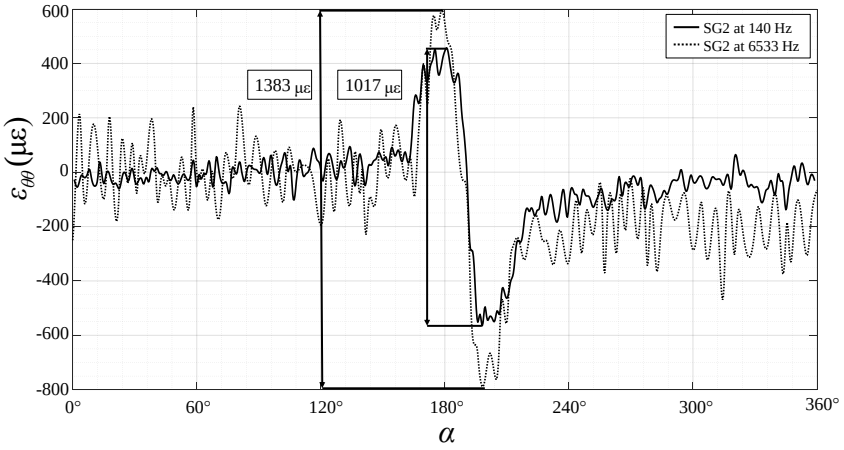

Figure 4: Strain gauge 2: comparison between the "static" reference at 140 Hz and the signal acquired at 6533 Hz at the same torque.

3. Static model of the tested gears

A static analysis is required in order to calculate the parameters needed to set up the dynamic model described in Section 4 and to verify that the tooth root strains measured at a meshing frequency 140 Hz are representative of the nominal torque transmitted between the meshing pair. This analysis was carried out by means of an elastic finite element model with generalized plane-strain 2-D elements in which a not-linear unilateral contact between the mating teeth was considered. An angular sector, large enough to cover at least one meshing cycle, was used to reproduce the tested gears: one sector was fixed at its hub, whilst the other was constrained by a hinge on the axis of its shaft and loaded by the nominal (mean) torque M. The contact between the gear pair was modeled using contact and target elements, with a friction coefficient of 0.2. The local hoop strain in the tooth fillet was measured in a cylindrical coordinate system, and the numerically simulated reading of all the strain gauges was obtained by integrating the hoop strain on the region of the gauge grid.

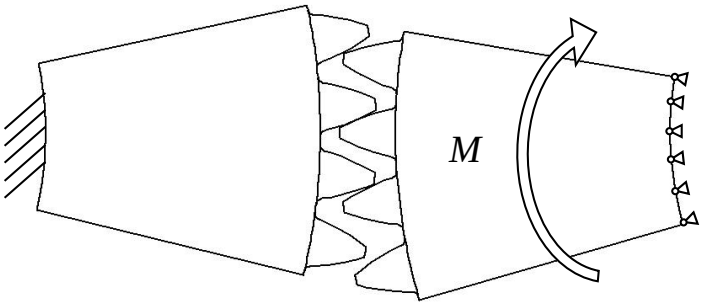

(a)

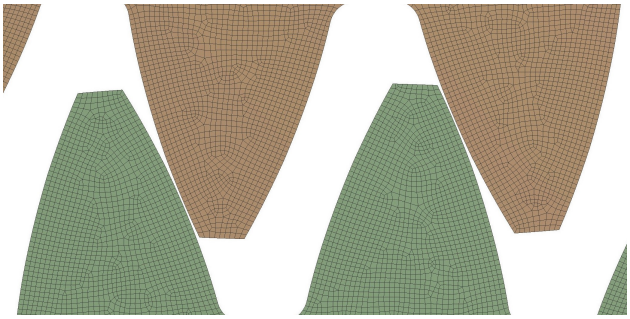

(b)

Figure 5: Finite elements model. (a) Scheme. (b) Mesh used.

The mesh size was chosen to take into account all the effects that could influence the parameters required for the dynamic model:

- A convergence analysis was conducted on the maximum contact pressures and hub displacements obtained.
- The mesh size used for the gears teeth was compared with the theoretical contact radius, and the best results were found for a 0.125 mm mesh (six times smaller than the theoretical contact radius predicted using the Hertzian theory).

Figure 6 compares the measured signal and the simulated strain calculated by the finite element model for a complete gear turn. The measured peak-to-peak hoop strain was 1017 $\mu\varepsilon$, whilst the simulated value was 1022 $\mu\varepsilon$. A relative difference not exceeding 0.5% confirms the validity of the model in reproducing the static behavior of the gears, and demonstrates that a meshing frequency of 140 Hz can be considered low enough to neglect any dynamic effects.

The same comparison is made at 6533 Hz in Figure 7. At 6533 Hz, the load transmitted by the meshing teeth is expected to be affected by the vibration and, as a consequence, the torque applied to the gear hub was obtained by multiplying the nominal (mean) value by the dynamic overload factor K_V measured in that regime. In this case, there was a relative difference of 0.4%, thus indicating that the overload detected experimentally is due an increase in the torque transmitted by the gears as a consequence of the dynamic conditions.

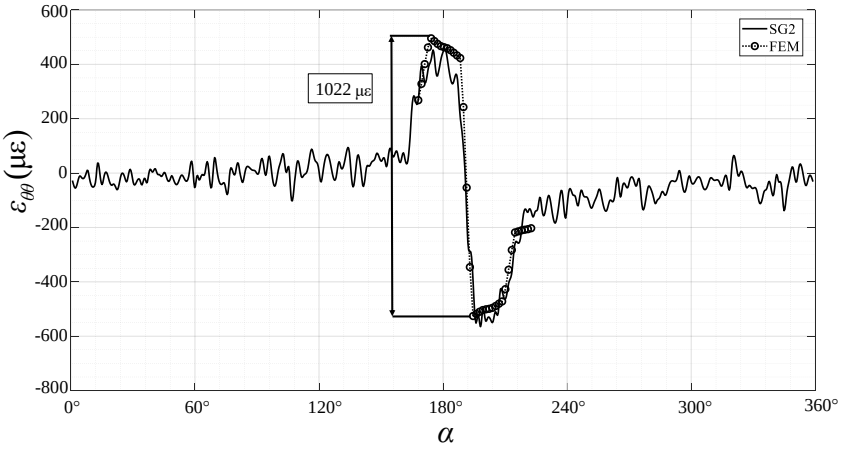

Figure 6: Hoop strain at the tooth root: comparison between experimental results and finite element calculation (static analysis with the nominal torque) at 140 Hz.

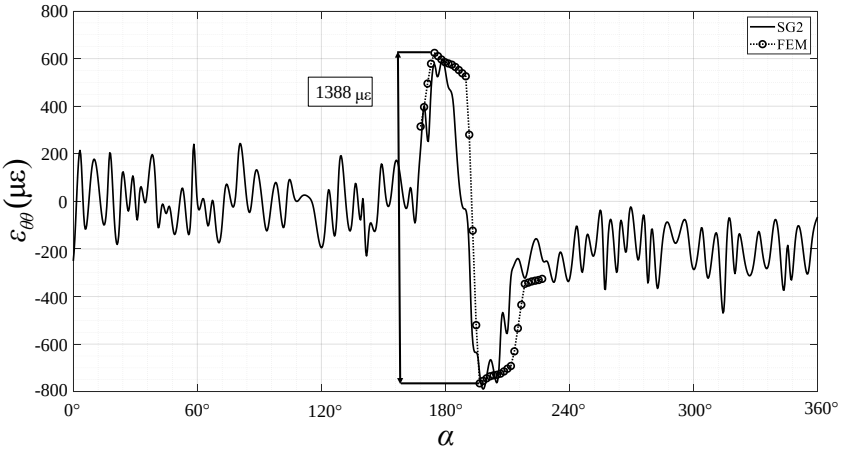

Figure 7: Hoop strain at the tooth root: comparison between experimental results and finite element calculation (static analysis with the nominal torque increased by the measured K_V factor) at 6533 Hz.

4. Dynamic model of the rig

The layout in Figure 1 inspired us to develop a lumped parameter model to study the dynamic behavior of the whole rig (Figure 8). The number of degrees of freedom, 17 in total, was selected in order to obtain a satisfactory agreement with the experimental results. The the angular coordinates θ_i were chosen in the same direction for each element.

Only rotational degrees of freedom for the inertial elements were modeled, as no bending-torsional coupling was considered. This assumption is justified by the test rig design that required very stiff shafts and bearings supporting the gears. Element 1 is the electrical engine, elements 2, 7, 8, 9, 10, 13, 14, 15 and 16 are joints, and the remaining inertial elements are gears. In the dynamical model, the inertial elements are connected by torsional springs and dampers in parallel, whose parameters were calculated taking into account the torsional stiffnesses of shafts and joints, and by using two different damping ratios depending on the kind of element

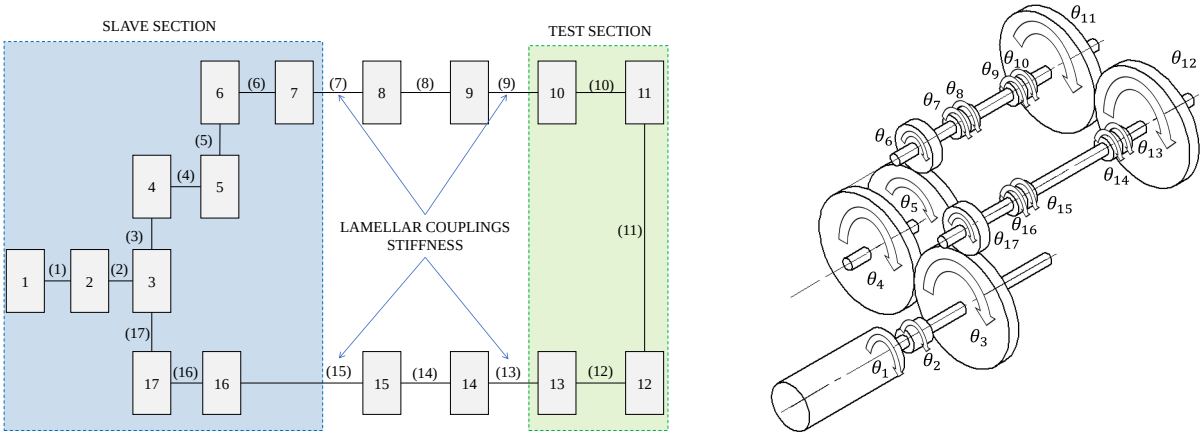

(a) (b)

Figure 8: Lumped parameter model. (a) 2-D scheme with the inertial elements i and their connecting springs/dampers (i), with $i = 1..17$. (b) 3-D scheme with the definition of the Lagrangian angular coordinates θ_i for any inertial element.

considered. The damping ratio ζ for the engaging gears was chosen on the basis of similar analyses found in the literature. Umezawa et al. [25, 26] and Cai and Hayashi [13] suggested a value of $\zeta = 0.07$, whereas Özgüven and Houser [1] used $\zeta = 0.1$ for their numerical simulation. We opted for a damping ratio of 0.05 for the engaging gears. In additions, since the dissipation effects are concentrated in those connections, a damping ratio of 0.001 was assumed for all the remaining links of the system.

4.1. Modeling the contact between engaging gears

In the conditions reproduced by the test rig, the connection between the engaging gears under test (11 and 12) are the only significant sources of anomalies in the motion which induce the dynamic effects in the system. As a lumped parameter model was adopted, the process of force transfer between the engaged gears was modeled (Figure 9) [1, 5, 6] by means of a spring with stiffness $k_{\mathrm{m}}(t)$ (the subscript "m" refers to meshing) representing the meshing stiffness, in series with a clearance b representing the gear backlash. The stiffness $k_{\mathrm{m}}(t)$ depends on the current contact configuration and, consequently, given the rotational speed, it can be represented as a function of the time. In parallel with the spring and the clearance element, a damper c_{m} was considered. This means that the power loss due to the friction mediated by the lubricant, the internal material dissipation and the kinetic energy loss in impacts due to the start of the meshing was taken into account by means of a global parameter. In order to reproduce the tooth profile (with the tip relief), the static transmission error $e(t)$ was introduced into the contact model using an error generator that creates a periodic time-dependent (or configuration-dependent) relative displacement between the engaging teeth along the line of contact.

For each pair of engaging gears, R_{bp} and R_{bg} (the base radii) and θ_{bp} and θ_{bg} (the angle of rotation of gear

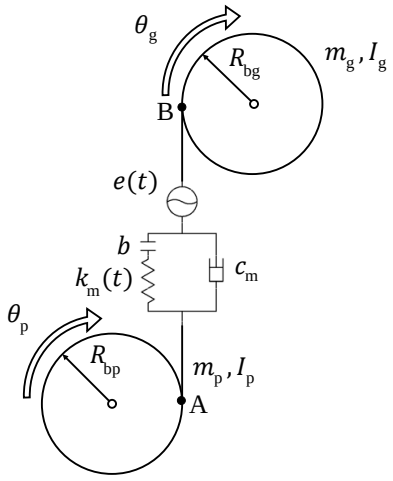

Figure 9: The gear connection. Subscripts "p" and "g" indicate the gear and the pinion, respectively.

and pinion, respectively) are defined first. The exchanged meshing force $F(t)$ is then defined by the following equations:

$$F(t) = \begin{cases} k_m(t)[u(t) - b] & \text{if} \quad u \geq b \\ 0 & \text{if} \quad |u| < b \\ k_m(t)[u(t) + b] & \text{if} \quad u \leq -b \end{cases}$$

$$u(t) = R_{bp}\theta_{bp} + R_{bg}\theta_{bg} - e(t)$$

in which $u(t)$ indicates the relative displacement between points A and B in Figure 9 (i.e. the relative displacement between the gears measured along the line of contacts).

As the slave section was designed with oversized components, in particular helical gears with 1:3 speed ratio, the contacts are more precise and regular than those between the tested gears. The mean meshing stiffness of the gear pairs of the slave section is at least 10 times higher than the stiffness of the tested gears, while their rotational inertia is 100 times higher (see Appendix A). The gears in the slave section operate in conditions of higher torque and lower angular speed compared to the tested gears. As a consequence, in the slave section, the effects of the static transmission error and of the backlash were neglected. The contact between engaging gears was thus modeled without time-dependent parameters by an ideal (constant) spring and a damper placed in parallel on the line of contacts.

4.2. Meshing stiffness and static transmission error calculation

The meshing stiffness variation versus time (or versus the relative gear angular position) of the tested gears significantly affects vibration and has to be modeled to ensure accurate dynamic evaluations. The meshing

stiffness depends on many factors, including the geometry of the tooth (nominal and effective) and the level of transmitted torque. Accurate modeling entails taking into account the variation in stiffness due to the varying number of the effectively engaged couples of teeth (one or two), the varying position of the contact region along the tooth profiles, and the non-linearity induced by the Hertzian contact.

We used the finite element model proposed in Section 3 to include all the above mentioned effects in the calculation of the total meshing stiffness $k_{\mathrm{m}}(t)$ in a single meshing period T. The model was used to evaluate the relative gear rotations at their hubs $\Delta\theta$ when a torque M is applied at any roll angle. In this case, the linear meshing stiffness in the direction of the line of contacts can be calculated as:

$$k_{\mathrm{m}}(\phi_j) = \frac{M}{R_{\mathrm{b}}^2 \Delta\theta(\phi_j)}$$

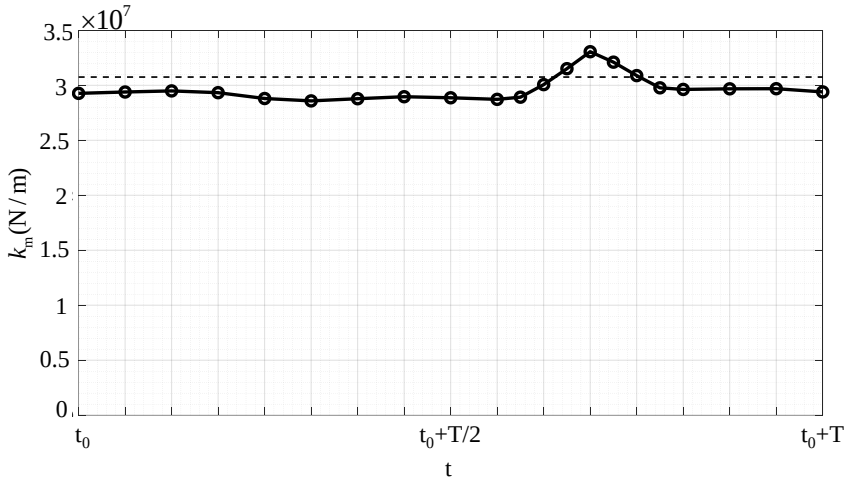

Figure 10: Time varying meshing stiffness at a mean torque equal to 150 Nm.

Figure 10 plots the calculated global stiffness obtained vs time and compares it with the midrange $\bar{K}$, in this condition equal to 30.8 MN/m.

The transmission error quantifies the difference between the real and ideal relative teeth displacement of two mating gears along the line of contacts. The error results from the profile modifications, the effective meshing stiffness, and the applied torque. When this quantity is measured (or calculated) at a low angular speed, it is defined as a static transmission error which only depends on the torque.

In our study, the static transmission error represents the main cause of excitation for the vibration. In fact, it acts similarly to a varying torque with the period of the meshing superimposed on the mean torque applied. Its trend in a meshing cycle was obtained using the static model described in Section 3. In these conditions, the static transmission error is calculated by multiplying the rotation of the loaded gear and its base radius. The

results obtained are shown in Figure 11.

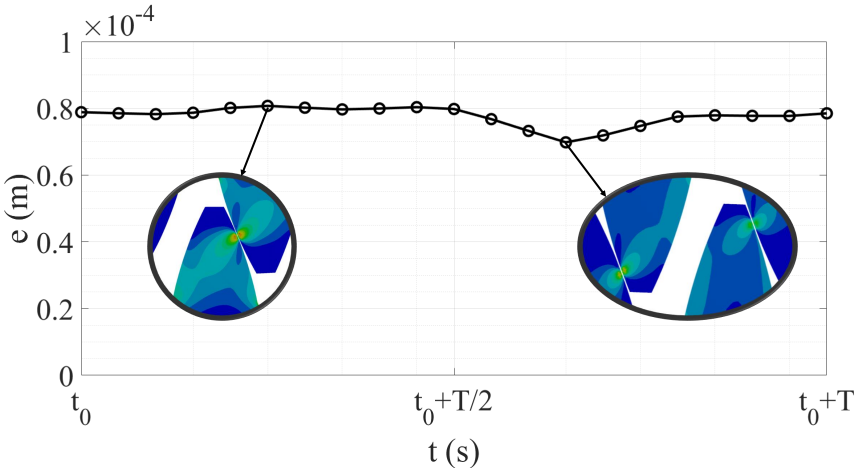

Figure 11: Static transmission error at a mean torque equal to 150 Nm.

5. Modal analysis

The system of equations (Appendix A) was used to evaluate the natural frequencies of the test rig and their related natural modes. In the modal analysis, damping was neglected. The effects of the time varying meshing stiffness were considered using a parametric study. The natural frequencies of the system were calculated by adopting the standard approach and the chart in Figure 10. The equations of motions were brought in a classical form (with only elastic and inertial contributions), the meshing stiffness of the tested gears was set to a constant value. The natural frequencies of the rig were calculated using three different values of the meshing stiffness of the tested gears in order to be representative of its range in the whole meshing cycle. In Table 1, the results refer to the mean meshing stiffness at different torques. In Table 2, the results in the different columns refer to the maximum, the minimum and the mean meshing stiffness at 150 Nm. If those different values of k_m are considered, at a certain torque level, a slight variation in the evaluated natural frequencies of the rig is produced. However, this effect is limited to a few modes and the relative differences are within a few percentage points. In particular, the highest and lowest natural frequencies and all the modal shapes were not affected by the stiffness variations. Consequently, the natural frequencies of the system and their related eigenvectors can be accurately estimated using the mean meshing stiffness.

Similar conclusions can be drawn considering three different torque levels (150 Nm, 500 Nm and 1000 Nm), for which there is a difference in the mean meshing stiffness k_m: none of the natural modes are changed, and the variation produced in the natural frequencies of the system is negligible. These results were also verified experimentally. The modal analysis was used to select, for the endurance tests, rotational speeds in "safe"

intervals for all the test rig components, thus avoiding all the possible regimes of resonance of the rig.

Mode	**f (Hz), 150 Nm**	**f (Hz), 500 Nm**	**f (Hz), 1000 Nm**
1	0	0	0
2	51	51	51
3	395	395	395
4	661	672	672
5	857	1028	1028
$6^{(*)}$	1208	1224	1224
7	1294	1294	1294
$8^{(*)}$	1505	1531	1531
$9^{(*)}$	1587	1612	1614
$10^{(*)}$	1761	1772	1772
$11^{(*)}$	1886	1889	1889
12	2589	2589	2589
$13^{(*)}$	2647	2710	2710
14	3031	3031	3031
15	3610	3610	3610
16	4322	4322	4322
17	4326	4326	4326
$\bar{K}$	30.8 MN/m	108 MN/m	110.9 MN/m

Table 1: Natural frequencies calculated using the mean meshing stiffness. Modes varying with the meshing stiffness are highlighted (*).

Mode	**f (Hz) at $\bar{K}$**	**f (Hz) at $K_{\max}$**	**f (Hz) at $K_{\min}$**
6	1208	1209	1207
8	1505	1508	1503
9	1587	1589	1586
10	1761	1762	1761
11	1886	1886	1886
13	2647	2652	2642
$\bar{K}$	30.8 MN/m	33.1 MN/m	28.6 MN/m

Table 2: Natural frequencies in a meshing cycle at 150 Nm of nominal torque.

6. Integration algorithm

The equations of motion (Appendix A) with the time-dependent parameters were integrated to obtain the dynamic response of the whole system when the rig is in under test conditions. The proposed algorithm (Figure 12) was used to simulate the tests performed on the rig, namely:

- Vibration surveys: the angular velocity of the tested gears was increased at a constant rate, thus increasing the meshing frequency from 1400 Hz to 9800 Hz in 4 minutes.
- Endurance tests: steady state conditions were kept for a long time in order to characterize the durability of the tested gears in typical operative conditions.

Following Shampine and Reichelt [27], a numerical study of the integration scheme was conducted in order to ensure accurate results. As the main result of this study, the ODE 113 (Adams-Bashfort-Moulton) was considered the best choice to characterize the dynamic behavior of the system. A maximum relative integration tolerance of

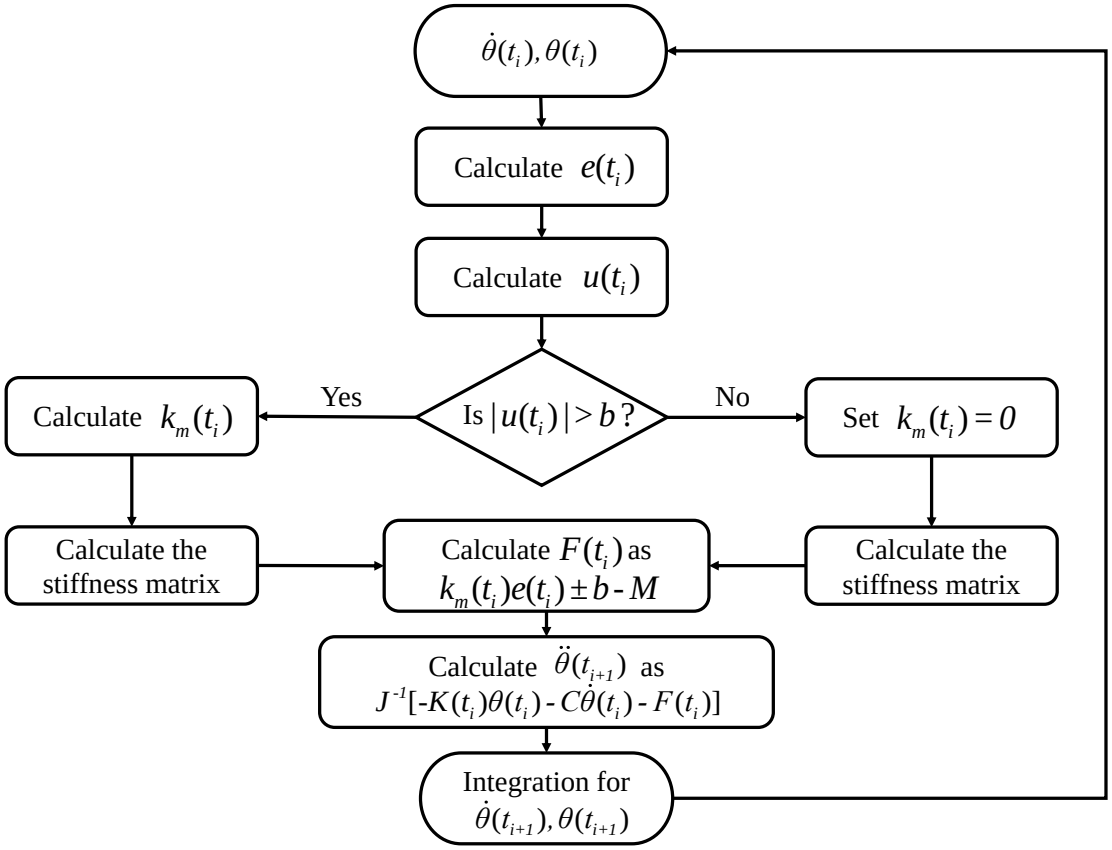

Figure 12: Integration scheme.

10^{-6} was chosen for the transients (vibration survey analyses) and a maximum relative integration tolerance of 10^{-3} was chosen for the steady states (endurance test analyses).

7. Simulation results

We verified numerically that if the time interval required to reach the maximum rotational speed is longer than 10 seconds, it has a negligible effect on the results. As a consequence, an interval of 15 seconds was chosen to simulate the vibration surveys under a constant torque of 150 Nm.

By considering the results of the simulated vibration surveys, it is possible to calculate the estimated frequency response function (FRF) of the system using Welch's algorithm. In particular, figure 13 represents the FRF of the total displacement along the line of contacts of the tested gears as a function of the meshing frequency together with the stability of the relevant modes obtained. The most dangerous resonance peak is located at a meshing frequency of 2613 Hz, and its nonlinear features were highlighted by simulating the response of the system at that meshing frequency after imposing an initial displacement from the dynamic equilibrium condition (θ_0). The variation of parameters like the damping ratio of the tested gears, the preload torque, and the initial displacement applied allowed a further analysis of the dynamic behavior of the system.

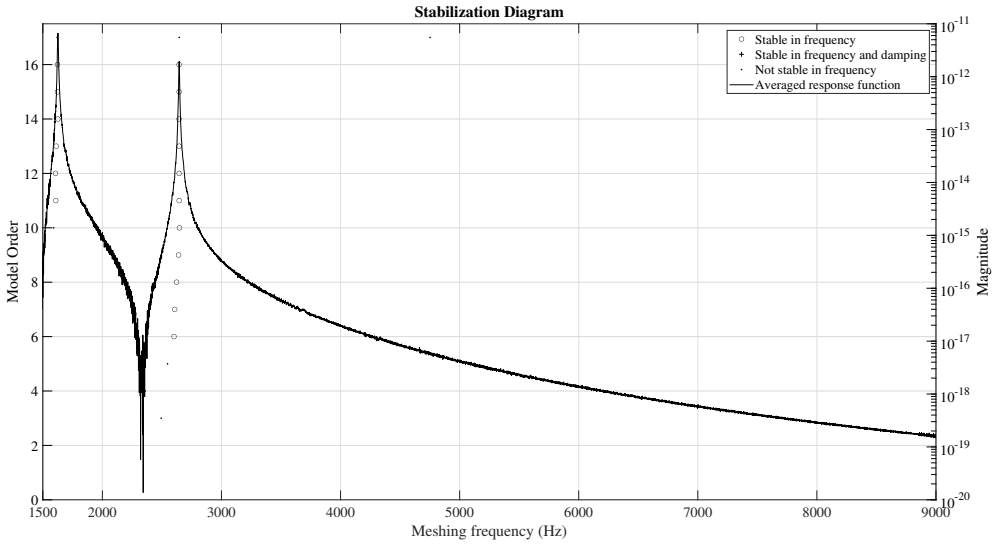

Figure 13: Stabilization diagram, $\zeta = 0.05$

As shown in figures 14, 15, the resonance at 2613 Hz is stable since the distance of the system's trajectories from the dynamic equilibrium condition is limited for a certain damping value. Furthermore, depending on the damping ratio chosen for the simulation of the tested gears, the system's trajectories can converge to the dynamic equilibrium condition, thus the resonance can be asymptotically stable.

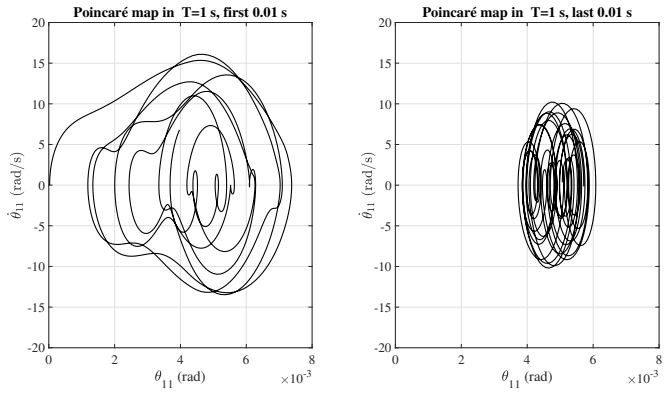

(a)

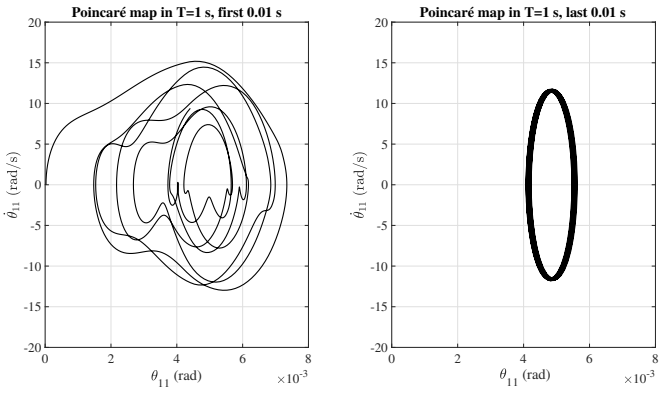

(b)

Figure 14: Poincaré maps obtained by varying ζ at 2613 Hz. (a) $\zeta = 0.001$. (b) $\zeta = 0.015$.

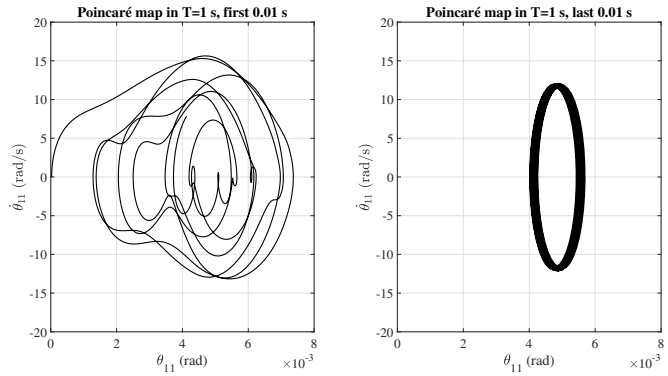

(a)

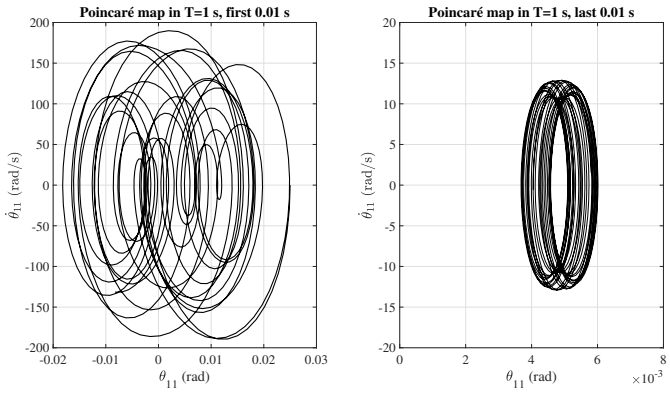

(b)

Figure 15: Poincaré maps obtained by varying $\theta(0)$ at 2613 Hz ($\zeta = 0.005$). (a) $\theta(0) = \theta_0$. (b) $\theta(0) = 1000\theta_0$.

By reducing the preload torque only, a new branch of periodic motion can be obtained: if the preload torque is not high enough, the gears teeth are characterized by an identical vibration and the Poincaré maps similar to the ones previously presented (though scaled), however the gear teeth are not in contact.

To verify the reliability of the model, the dynamic response of the system was simulated using a low damping ratio (ζ=0.01) in order to highlight the resonance conditions. The outcomes of the model (angular displacements, velocities and accelerations) were directly compared with the signals detected by the accelerometers installed on the rig. The model results are in good agreement with the experimental outcomes. Except for the low frequency resonances (below a meshing frequency of 1400 Hz), which are outside of the test range and have a negligible effect on the dynamic overload for the tested gears, the model predicts the resonances at a meshing frequency of 2473 Hz and 3733 Hz (figure 16), and with a relative error of about 5%. The spectral content of the experimental signal was also correctly reproduced by the model (figure 17). A difference was observed only at 7467 Hz, a regime in which a resonance detected experimentally was not determined by the model. This inability of the model could be justified by a possible bending torsional-coupling mode, which is not unlikely at that high frequency which is not included in the model.

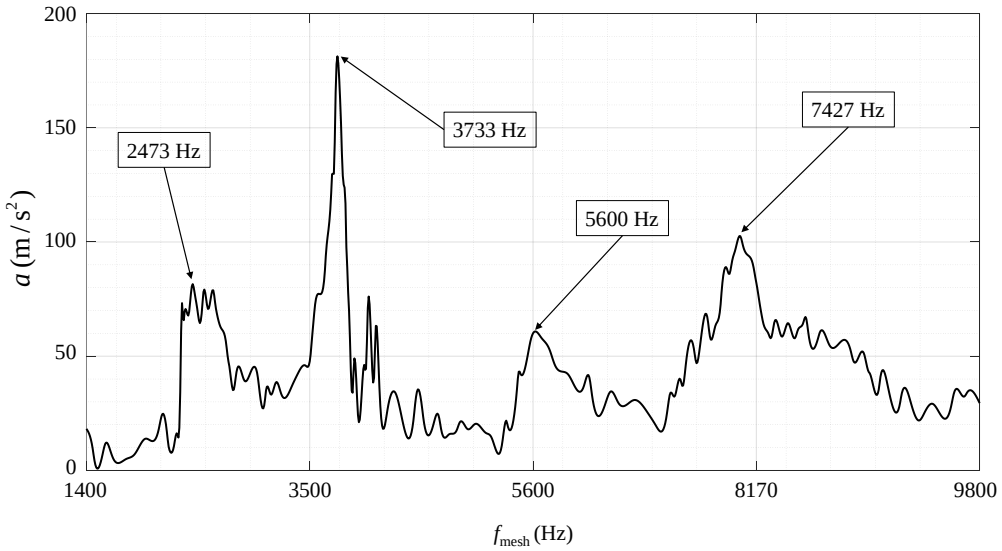

Figure 16: Detection of experimental resonances using the accelerometer signal as a function of the meshing frequency.

Experimental resonance	Simulated resonance	Relative Difference
2473 Hz	2613 Hz	5.3 %
3733 Hz	3724 Hz	-0.25 %
5600 Hz	5740 Hz	2.5 %
7467 Hz	Not predicted	-

Table 3: Experimental and calculated resonances.

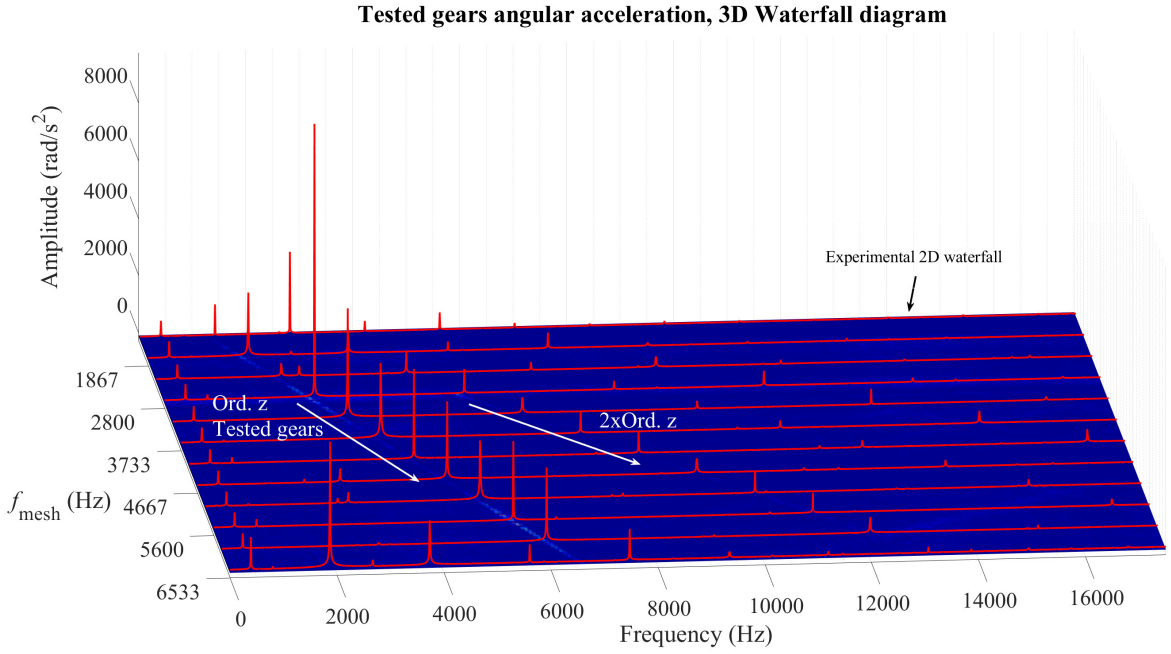

Figure 17: The simulated and the experimental acceleration signal as a function of the meshing frequency. The first two harmonics of the meshing gears are highlighted.

No contact loss between the tested gears was foreseen at the gear working speed (equivalent to 6533 Hz). This result was confirmed experimentally by analyzing the strain gauge signals (resulting in a pulsating output during a complete rotation of the gears, when a lower torque is applied). Moreover, by considering different values of ζ (between 0.01 and 0.1), we verified that the influence of (low) damping on the natural frequencies of the system can be neglected. No peaks are observed in the dynamic response of the system if the meshing frequency of the tested gears is above 2800 Hz. The resonances at 3733 Hz and 5600 Hz do not produce significant effects if a $\zeta \geq 0.01$ is chosen for the simulation. How the damping ratio affects the solution can be quantified by considering the main resonance peaks for a meshing frequency of between 1400 Hz and 3733 Hz. As shown in figure 18, contact loss is present only when $\zeta \leq 0.005$ is chosen for the simulation. In all the other cases (as already stated), the damping ratio chosen does not affect the resonance frequencies identified and only dampens the resonance peaks found. For example, increasing ζ from 0.015 to 0.03 just causes a 10% reduction in the dynamic overload factor at 2613 Hz.

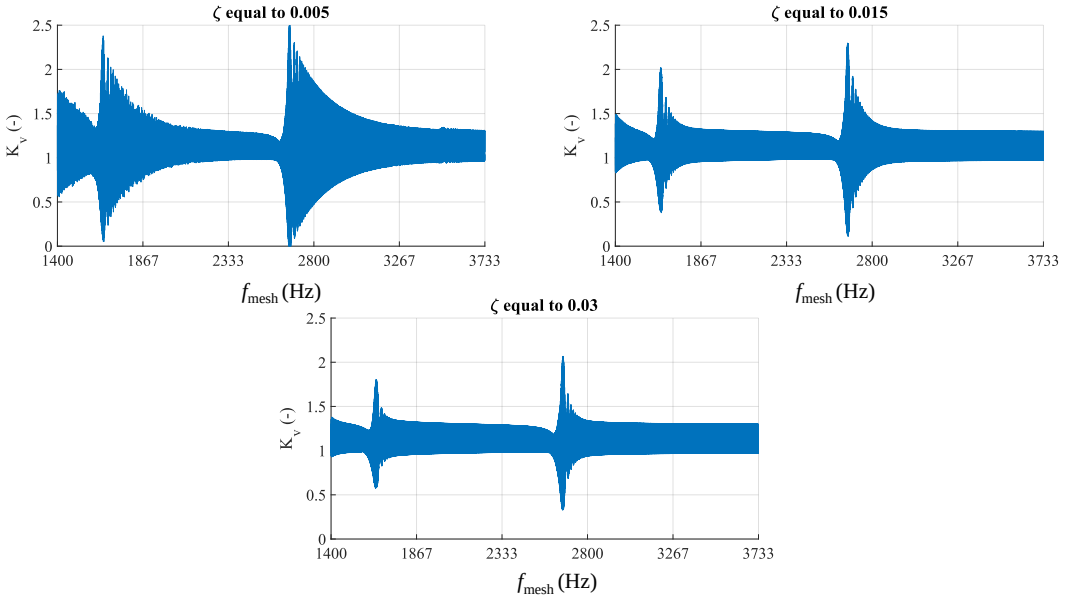

Figure 18: Damping ratio effects on the resonance peaks between 1400 and 3733 Hz.

Regarding the different values of the static transmission error of the tested gears (with the same meshing stiffness and damping), as expected, changing the excitation amplitude (though maintaining its shape) does not modify the resonance frequencies of the rig, but modifies the amplitude of the response of the system (figure 19). The most intense peak at a meshing frequency of 2613 Hz increases by about 0.2 (in terms of dynamic overload factor) for each increase in the static transmission error (each increment is of 0.5 times the initial static transmission error considered), until contact loss is experienced for $e(t) = 3e_0(t)$ (where $e_0(t)$ is the initial static transmission error

considered).

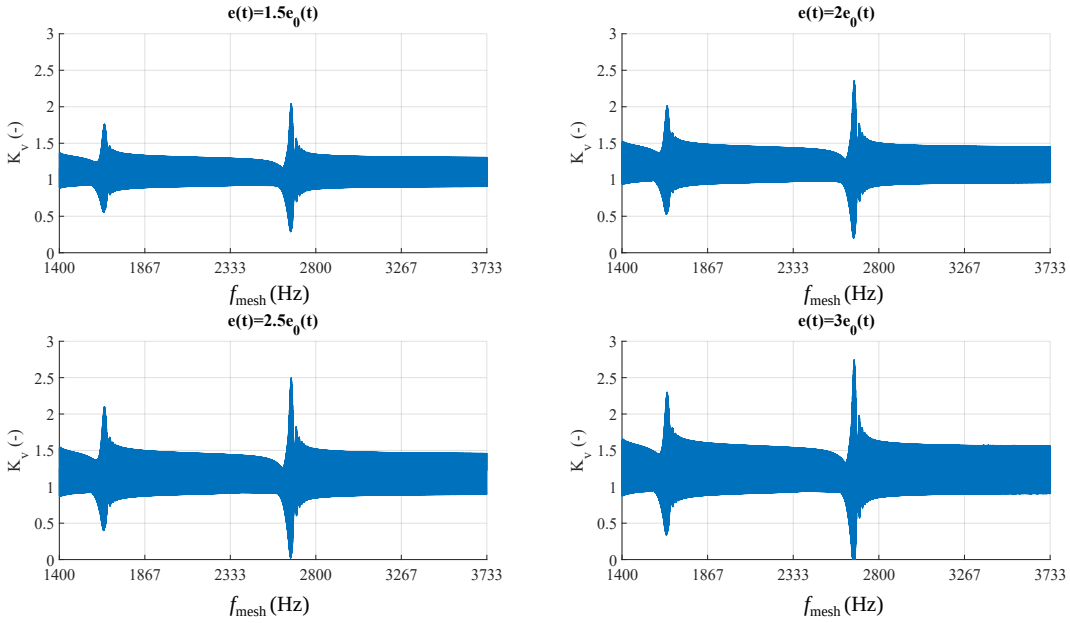

Figure 19: Static transmission error effects on the resonance peaks between 1400 and 3733 Hz.

The dynamic overload factor was measured at a meshing frequency of 6533 Hz using the (redundant) signals acquired through the strain gauges: one such signal is plotted in Figure 4. The value of K_V was 1.36, which was obtained as the ratio between the peak-to-peak signals at 6533 Hz and at 140 Hz (quasi-static value). Even though a low damping ratio was used for the simulation (equal to 0.05), the calculated value of K_V was equal to 1.33. The relative difference between the simulated and the experimental value is about 2%. It is worth noting that the dynamic overload factors obtained by the model were significantly different from those derived using the ISO 6336-B[28]. Even though those values were identical in terms of the resonance of the gear pair (located at 1307 Hz in a single degree of freedom model), the most dangerous peak cannot be obtained if a model that only includes the tested gears is considered. This highlights the importance of modeling the dynamical behavior of the whole transmission system in the evaluation of K_V of a single gear pair.

For the transmission under study, the maximum value of the dynamic overload factor, with a nominal torque of 150 Nm, is equal to 1.81 and is produced at 2613 Hz, which is 50% higher than the quantity evaluated by the ISO standard (figure 20). The dynamic overload factor calculated for the endurance tests at 6533 Hz (far from any resonance frequencies) is 1.33 which is in fairly good agreement with the experimentally obtained value. At 6533 Hz, the K_V suggested by the standard is 1.

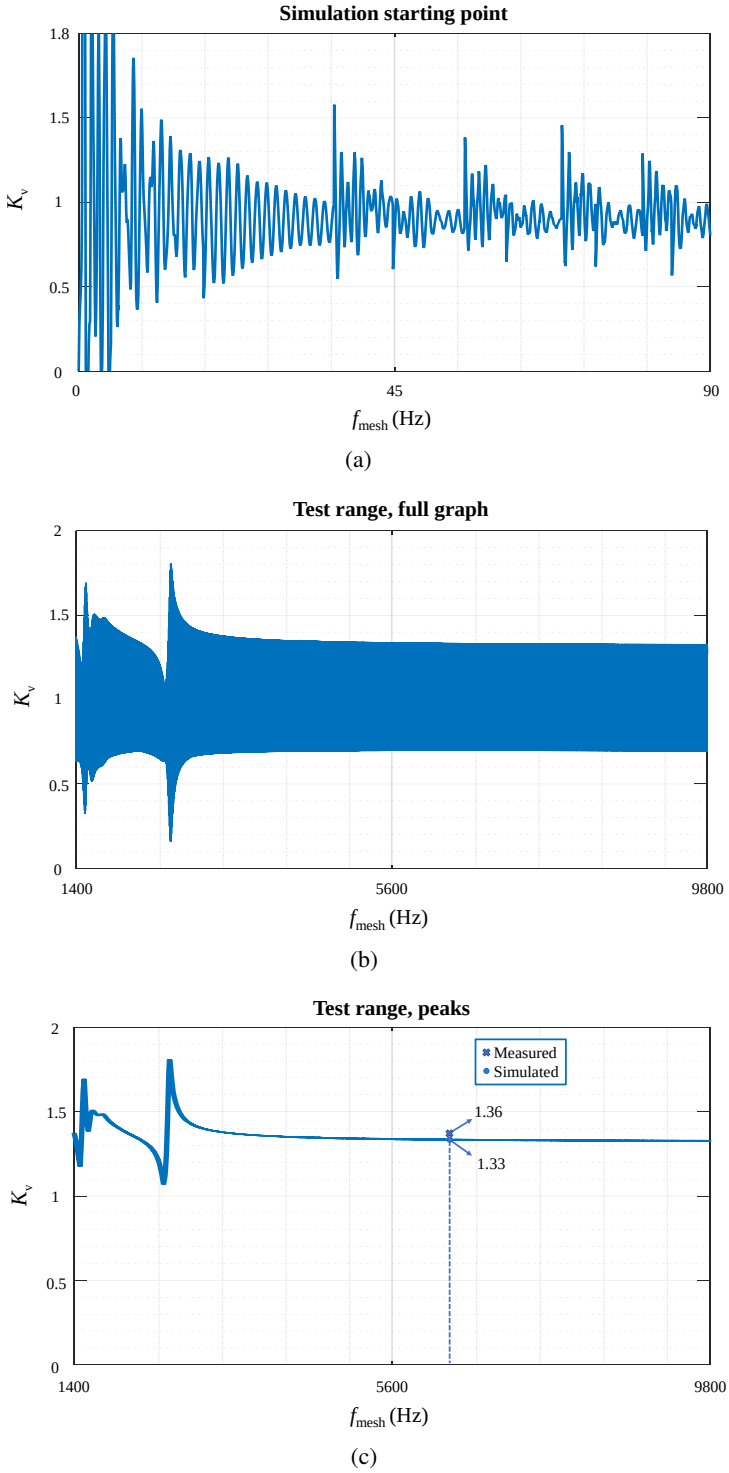

Figure 20: Dynamic overload factor of mesh force simulated in the testing range as a function of the meshing frequency (150 Nm of applied torque). (a) Simulation starting point. (b) Test range, full graph. (c) Test range, peaks.

8. Conclusions

We have presented two models for evaluating the dynamical behavior of a mechanical power recirculating rig. We used a (static) finite element model to obtain the time/configuration varying quantities that characterize the

tested gears. The same model was used to verify the absence of dynamic effects on the strain gauge signals when low angular speeds are applied. On the other hand, in order to evaluate the dynamic behavior of the transmission in its rather wide range of operative conditions, we used a lumped parameter model to allow for a more in-depth characterization of the nonlinear dynamics of the system. This model required a numerical analysis in order to obtain an accurate time integration of the equations.

The frequency response function of the tested gears was numerically calculated using the simulated vibration surveys, and the nonlinear features of the most intense resonance peak were investigated using Poincaré maps. The variation of the "free" parameters of the rig (damping, initial displacement imposed, and preload torque) highlighted the stability of the resonance at a meshing frequency of 2613 Hz, and the presence of contact loss when the preload torque is not high enough.

By comparing the numerical results and the measured quantities, the proposed dynamic model was found to adequately reproduce the most significant dynamic phenomena of the transmission. In particular, the dynamic transmission error, the variations in the gear angular speed, and the dynamic overload factor were obtained for every test conditions (applied torque and angular speed) in reasonable processing times.

The simulation of the vibration survey was used to quantify the limits of the approach based on the commonly applied standards to evaluate resonance conditions. In the conditions considered, although the natural frequencies of the transmission could have been estimated by the traditional linear method based on the eigenvalues by assuming mean-values for the time varying parameters, only the complete dynamic simulation of the whole transmission actually identifies which resonances may be dangerous for the components. Furthermore, we found that if only the tested gears were considered, only one resonance frequency would be calculated and the dynamic overload factor would be significantly underestimated.

For the future, further experimental measurements in different operative conditions and the related simulations are programmed. These additional comparisons would be useful to identify more accurate values of the damping. We are also planning an upgrade of the lumped model so as to include some bending-torsional couplings of the transmission.

References

[1] H. N. Özgüven, D. R. Houser, Mathematical models used in gear dynamics—a review, Journal of Sound and Vibration 121 (3) (1988) 383–411.

[2] J. Wang, R. Li, X. Peng, Survey of nonlinear vibration of gear transmission systems, Applied Mechanics Reviews 56 (3) (2003) 309.

[3] C. H. Liou, H. H. Lin, F. B. Oswald, D. P. Townsend, Effect of contact ratio on spur gear dynamic load with no tooth profile modifications, Journal of Mechanical Design 118 (3) (1996) 439–443.

[4] J. H. Kuang, A. D. Lin, Theoretical aspects of toeque responses in spur gearing due to mesh stiffness variation, Mechanical Systems and Signal Processing 17 (2) (2003) 255–271.

[5] A. Kahraman, G. W. Blankenship, Effect of involute contact ratio on spur gear dynamics, Journal of Mechanical Design 121 (1) (1999) 112.

[6] A. Kahraman, G. W. Blankenship, Effect of involute tip relief on dynamic response of spur gear pairs, Journal of Mechanical Design 121 (2) (1999) 313.

[7] M. Beghini, F. Presicce, C. Santus, G. Bragallini, Influence of the linear tip relief modification in spur gears and experimental evidence, in: 12th International Conference on Experimental Mechanics, 2004.

[8] M. Beghini, F. Presicce, C. Santus, A method to define profile modification in spur gear and to minimize the transmission error, in: AGMA Fall Technical Meeting, 2004.

[9] M. B. Sánchez, M. Pleguezuelos, J. I. Pedrero, Influence of profile modifications on meshing stiffness, load sharing, and trasnsmission error of involute spur gears, Mechanism and Machine Theory 139 (2019) 506–525.

[10] Q. Chen, Y. Wang, W. Tian, Y. Wu, Y. Chen, An improved nonlinear dynamic model of gear pair with tooth surface microscopic features, Nonlinear Dynamics 96 (2) (2019) 1615–1634.

[11] T. Eritenel, R. G. Parker, Nonlinear vibration of gears with tooth surface modifications, Journal of Vibration and Acoustics 135 (5) (2013) 051005.

[12] R. W. Gregory, S. L. Harris, R. G. Munro, A method of measuring transmission error in spur gears of 1:1 ratio, Journal of Scientific Instruments 40 (1) (1963) 5–9.

[13] Y. Cai, T. Hayashi, The linear approximated equation of vibration of a pair of spur gears (theory and experiment), Journal of Mechanical Design 116 (2) (1994) 558.

[14] K. Ichimaru, F. Hirano, Dynamic behavior of heavy-loaded spur gears, Journal of Engineering for Industry 96 (2) (1974) 373.

[15] M. Amabili, A. Rivola, Dynamic analysis of spur gear pairs: steady-state response and stability of the SDOF model with tyme-varying meshing damping, Mechanical Systems and Signal Processing 11 (3) (1997) 375–390.

[16] S. Theodossiades, S. Natsiavas, Non-linear dynamics of gear-pair systems with periodic stiffness and backlash, Journal of Sound and Vibration 229 (2) (2000) 287–310.

[17] T. Eritenel, R. G. Parker, An investigation of tooth mesh nonlinearity and partial contact loss in gear pairs using a lumped-parameter model, Mechanism and Machine Theory 56 (2012) 28–51.

[18] E. Sakaridis, V. Spitas, C. Spitas, Non-linear modeling of gear drive dynamics incorporating intermittent tooth contact analysis and tooth eigenvibrations, Mechanism and Machine Theory 136 (2019) 307–333.

[19] D. Xiang, Y. Shen, Y. Wei, A contact force model considering meshing and collision states for dynamic analysis in helical gear system, Chinese Journal of Mechanical Engineering 32 (1).

[20] Z. Zhu, L. Cheng, R. Xu, R. Zhu, Impacts of backlash on nonlinear dynamic characteristic of encased differential planetary gear train, Shock and Vibration 2019 (2019) 1–15.

[21] J. Shi, X. Gou, L. Zhu, Modeling and analysis of a spur gear pair considering multi-state mesh with time-varying parameters and backlash, Mechanism and Machine Theory 134 (2019) 582–603.

[22] J. Wang, J. Zhang, Z. Yao, X. Yang, R. Sun, Y. Zhao, Nonlinear characteristics of a multi-degree-of-freedom spur gear system with bending-torsional coupling vibration, Mechanical Systems and Signal Processing 121 (2019) 810–827.

[23] C. Su, S. Wang, Y. Liu, P. Dong, X. Xu, Coupled vibrations of a drive system during automatic transmission, Advances in Mechanical Engineering 11 (3) (2019) 168781401983350.

[24] M. Amorena, G. M. Bragallini, S. Manconi, E. Manfredi, M. Vitali, Characterization of aerospace gears by high speed testing, in: International Conference on Gears, 2005.

[25] K. Umezawa, T. Ajima, H. Houjoh, Vibration of three axes gear system, Bulletin of JSME 29 (249) (1986) 950–957.

[26] K. Umezawa, T. Sato, J. Ishikawa, Simulation of rotational vibration of spur gears, Bulletin of JSME 27 (223) (1984) 102–109.

[27] L. F. Shampine, M. W. Reichelt, The MATLAB ODE suite, SIAM Journal on Scientific Computing 18 (1) (1997) 1–22.

[28] ISO-6336, Calculation of Load Capacity of Spur and Helical Gears (2006).

Appendices

A. Equations of motion and numerical parameters

For the sake of completeness, the system of equations used to characterize the rig is reported hereafter using the relative matrices. The subscripts are referred to the element order shown in figure 8. It should be noted that, for the reasons discussed in section 4, the equations of the elements 11 and 12 are the only ones containing a time varying stiffness and a time varying transmission error.

From the equations of motion, we obtain that:

$$M\ddot{\theta} + C\dot{\theta} + K\theta = F$$

$$M = \mathrm{diag}(J_1, J_2, ..., J_n)$$

$$K = \begin{pmatrix}
k_1 & -k_1 & 0 & 0 & 0 & 0 & 0 & 0 & 0 & 0 & 0 & 0 & 0 & 0 & 0 & 0 & 0 \\
-k_1 & k_1+k_2 & -k_2 & 0 & 0 & 0 & 0 & 0 & 0 & 0 & 0 & 0 & 0 & 0 & 0 & 0 & 0 \\
0 & -k_2 & k_2+k_3 r_{b3}^2 + k_{17} r_{b3}^2 & 0 & 0 & 0 & 0 & 0 & 0 & 0 & 0 & 0 & 0 & 0 & 0 & 0 & k_{17} r_{b3} r_{b17} \\
0 & 0 & k_3 r_{b3} r_{b4} & k_4 r_{b4}^2 & -k_4 & 0 & 0 & 0 & 0 & 0 & 0 & 0 & 0 & 0 & 0 & 0 & 0 \\
0 & 0 & 0 & -k_4 & k_4 + k_5 r_{b5}^2 & k_5 r_{b5} r_{b6} & 0 & 0 & 0 & 0 & 0 & 0 & 0 & 0 & 0 & 0 & 0 \\
0 & 0 & 0 & 0 & k_5 r_{b5} r_{b6} & k_6 + k_5 r_{b6}^2 & -k_6 & 0 & 0 & 0 & 0 & 0 & 0 & 0 & 0 & 0 & 0 \\
0 & 0 & 0 & 0 & 0 & -k_6 & k_6+k_7 & -k_7 & 0 & 0 & 0 & 0 & 0 & 0 & 0 & 0 & 0 \\
0 & 0 & 0 & 0 & 0 & 0 & -k_7 & k_7+k_8 & -k_8 & 0 & 0 & 0 & 0 & 0 & 0 & 0 & 0 \\
0 & 0 & 0 & 0 & 0 & 0 & 0 & -k_8 & k_8+k_9 & -k_9 & 0 & 0 & 0 & 0 & 0 & 0 & 0 \\
0 & 0 & 0 & 0 & 0 & 0 & 0 & 0 & -k_9 & k_9+k_{10} & -k_{10} & 0 & 0 & 0 & 0 & 0 & 0 \\
0 & 0 & 0 & 0 & 0 & 0 & 0 & 0 & 0 & -k_{10} & k_{10}+k_{11} r_{b11}^2 & k_{11} r_{b11} r_{b12} & 0 & 0 & 0 & 0 & 0 \\
0 & 0 & 0 & 0 & 0 & 0 & 0 & 0 & 0 & 0 & k_{11} r_{b11} r_{b12} & k_{12}+k_{11} r_{b12}^2 & -k_{12} & 0 & 0 & 0 & 0 \\
0 & 0 & 0 & 0 & 0 & 0 & 0 & 0 & 0 & 0 & 0 & -k_{12} & k_{12}+k_{13} & -k_{13} & 0 & 0 & 0 \\
0 & 0 & 0 & 0 & 0 & 0 & 0 & 0 & 0 & 0 & 0 & 0 & -k_{13} & k_{13}+k_{14} & -k_{14} & 0 & 0 \\
0 & 0 & 0 & 0 & 0 & 0 & 0 & 0 & 0 & 0 & 0 & 0 & 0 & -k_{14} & k_{14}+k_{15} & -k_{15} & 0 \\
0 & 0 & 0 & 0 & 0 & 0 & 0 & 0 & 0 & 0 & 0 & 0 & 0 & 0 & -k_{15} & k_{15}+k_{16} & -k_{16} \\
0 & 0 & k_{17} r_{b3} r_{b17} & 0 & 0 & 0 & 0 & 0 & 0 & 0 & 0 & 0 & 0 & 0 & 0 & -k_{16} & k_{17} r_{b17}^2 + k_{16}
\end{pmatrix}$$

$$C = \begin{pmatrix}
c_1 & -c_1 & 0 & 0 & 0 & 0 & 0 & 0 & 0 & 0 & 0 & 0 & 0 & 0 & 0 & 0 & 0 \\
-c_1 & c_1+c_2 & -c_2 & 0 & 0 & 0 & 0 & 0 & 0 & 0 & 0 & 0 & 0 & 0 & 0 & 0 & 0 \\
0 & -c_2 & c_2 + c_3 r_{b3}^2 + c_{17} r_{b3}^2 & 0 & 0 & 0 & 0 & 0 & 0 & 0 & 0 & 0 & 0 & 0 & 0 & 0 & c_{17} r_{b3} r_{b17} \\
0 & 0 & c_3 r_{b3} r_{b4} & c_4 r_{b4}^2 & -c_4 & 0 & 0 & 0 & 0 & 0 & 0 & 0 & 0 & 0 & 0 & 0 & 0 \\
0 & 0 & 0 & -c_4 & c_4 + c_5 r_{b5}^2 & c_5 r_{b5} r_{b6} & 0 & 0 & 0 & 0 & 0 & 0 & 0 & 0 & 0 & 0 & 0 \\
0 & 0 & 0 & 0 & c_5 r_{b5} r_{b6} & c_6 + c_5 r_{b6}^2 & -c_6 & 0 & 0 & 0 & 0 & 0 & 0 & 0 & 0 & 0 & 0 \\
0 & 0 & 0 & 0 & 0 & -c_6 & c_6+c_7 & -c_7 & 0 & 0 & 0 & 0 & 0 & 0 & 0 & 0 & 0 \\
0 & 0 & 0 & 0 & 0 & 0 & -c_7 & c_7+c_8 & -c_8 & 0 & 0 & 0 & 0 & 0 & 0 & 0 & 0 \\
0 & 0 & 0 & 0 & 0 & 0 & 0 & -c_8 & c_8+c_9 & -c_9 & 0 & 0 & 0 & 0 & 0 & 0 & 0 \\
0 & 0 & 0 & 0 & 0 & 0 & 0 & 0 & -c_9 & c_9+c_{10} & -c_{10} & 0 & 0 & 0 & 0 & 0 & 0 \\
0 & 0 & 0 & 0 & 0 & 0 & 0 & 0 & 0 & -c_{10} & c_{10}+c_{11} r_{b11}^2 & c_{11} r_{b11} r_{b12} & 0 & 0 & 0 & 0 & 0 \\
0 & 0 & 0 & 0 & 0 & 0 & 0 & 0 & 0 & 0 & c_{11} r_{b11} r_{b12} & c_{12}+c_{11} r_{b12}^2 & -c_{12} & 0 & 0 & 0 & 0 \\
0 & 0 & 0 & 0 & 0 & 0 & 0 & 0 & 0 & 0 & 0 & -c_{12} & c_{12}+c_{13} & -c_{13} & 0 & 0 & 0 \\
0 & 0 & 0 & 0 & 0 & 0 & 0 & 0 & 0 & 0 & 0 & 0 & -c_{13} & c_{13}+c_{14} & -c_{14} & 0 & 0 \\
0 & 0 & 0 & 0 & 0 & 0 & 0 & 0 & 0 & 0 & 0 & 0 & 0 & -c_{14} & c_{14}+c_{15} & -c_{15} & 0 \\
0 & 0 & 0 & 0 & 0 & 0 & 0 & 0 & 0 & 0 & 0 & 0 & 0 & 0 & -c_{15} & c_{15}+c_{16} & -c_{16} \\
0 & 0 & c_{17} r_{b3} r_{b17} & 0 & 0 & 0 & 0 & 0 & 0 & 0 & 0 & 0 & 0 & 0 & 0 & -c_{16} & c_{17} r_{b17}^2 + c_{16}
\end{pmatrix}$$

Excluding the eleventh and twelfth rows, F is a null vector. For the non null components:

$$F(11) = F(12) = M + k_{11}(t) R_{b,11}(e(t) + b)$$

In order to allow the reader to reproduce the results of the dynamic model proposed, the numerical values of the rotational inertia, of the stiffness and of the damping ratio considered (used for the final simulations) are presented in the following table.

D.O.F.	Rotational inertia (kgm^2)	Base radius (mm)	Connected elements	Stiffness	Damping ratio (-)
1	0.3000	-	1-2	0.0286 MNm/rad	0.001
2	0.0080	-	2-3	0.5004 MNm/rad	0.001
3	0.5950	172	3-4	1007.5 MN/m	0.050
4	0.6690	172	4-5	12.913 MNm/rad	0.001
5	0.7110	172	5-6	880.56 MN/m	0.050
6	0.0160	56	6-7	2.4913 MNm/rad	0.001
7	0.0095	-	7-8	0.1567 MNm/rad	0.001
8	0.0017	-	8-9	0.5295 MNm/rad	0.001
9	0.0017	-	9-10	0.1567 MNm/rad	0.001
10	0.0036	-	10-11	0.5263 MNm/rad	0.001
11	0.0063	64.5	11-12	30.800 MN/m	0.050
12	0.0063	64.5	12-13	0.5263 MNm/rad	0.001
13	0.0036	-	13-14	0.1567 MNm/rad	0.001
14	0.0017	-	14-15	0.5295 MNm/rad	0.001
15	0.0017	-	15-16	0.1567 MNm/rad	0.001
16	0.0125	-	16-17	1.0377 MNm/rad	0.001
17	0.0120	56	17-3	825.29 MN/m	0.050

Table 4: Numerical parameters.